Journal of Power Sources 240 (2013) 258–266

Contents lists available at SciVerse ScienceDirect

Journal of Power Sources

journal homepage: www.elsevier.com/locate/jpowsour

Enhanced proton conductivity under low humidity of sulfonated poly(ether ether ketone) composite membrane enabled by multifunctional phosphonic acid polymeric submicrocapsules

Lingli Nie [a], Hao Dong [a], Xi Han [a], Guangwei He [a], Hong Wu [a,b], Zhongyi Jiang [a,*]

[a] Key Laboratory for Green Chemical Technology of Ministry of Education, School of Chemical Engineering and Technology, Tianjin University, Tianjin 300072, China
[b] Tianjin Key Laboratory of Membrane Science and Desalination Technology, Tianjin University, Tianjin 300072, China

HIGHLIGHTS

- The phosphonic acid polymeric submicrocapsules are designed and synthetized.
- The submicrocapsules have multifunctions in water retention and proton transfer.
- The composite membranes exhibit high water uptake and water retention.
- The composite membranes exhibit high proton conductivity under low humidity.

ARTICLE INFO

Article history:
Received 25 December 2012
Received in revised form
31 March 2013
Accepted 3 April 2013
Available online 10 April 2013

Keywords:
Phosphonic acid polymeric submicrocapsule
Sulfonated poly(ether ether ketone)
Proton exchange membrane
Water retention
Proton conductivity

ABSTRACT

Phosphonic acid polymeric submicrocapsules (PASCs) are synthesized and incorporated into a sulfonated poly(ether ether ketone) (SPEEK) matrix to prepare composite membranes. The microstructure and physicochemical properties of the PASCs and the membranes are characterized by transmission electron microscopy (TEM), energy dispersive X-ray (EDX), field emission scanning electron microscope (FESEM), thermogravimetric analysis (TGA) and Fourier transform infrared spectroscopy (FTIR). Compared with the SPEEK control membrane, the PASC-filled composite membranes exhibit elevated water uptake and proton conductivity at 25 °C and 100% relative humidity (RH). The proton conductivity depends strongly on water content within the membranes. Under 40 °C and 20% RH, the composite membrane filled with 15 wt.% PASCs (128 nm lumen) shows the highest proton conductivity of 0.0142 S cm^{-1} after 90 min testing, about twelve times higher than that of the SPEEK control membrane (0.0011 S cm^{-1}), which is positively correlated with the water retention of the membrane. These results suggest that the PASC-filled composite membranes may find encouraging application as efficient water-retention and proton-conduction materials in proton exchange membrane fuel cells (PEMFCs).

1. Introduction

For a proton exchange membrane fuel cell (PEMFC), the membrane is a core and performance-determinant component, through which proton transfers from anode to cathode to fulfill the conversion of chemical energy into electrical energy [1]. Generally, proton transfers through a PEM via two principal mechanisms [2,3]: one is vehicle mechanism wherein proton diffuses as water-solvated species, such as H_3O^+, $H_5O_2^+$, $H_7O_3^+$ and $H_9O_4^+$; the other is Grotthuss mechanism wherein proton hops from one water molecule or functional group to the next by forming and breaking of hydrogen bonds. Accordingly, water in PEMs is vital to proton transfer and thus it is crucial to acquire membranes with high water retention, especially under low humidity [4,5].

To this end, various efforts have been devoted to enhancing water retention of PEMs, for example: (i) introducing abundant hydrogen-bonding sites for water molecules by incorporating hygroscopic fillers, such as solid, porous and hollow organic or inorganic fillers into membranes [6–15]; (ii) enhancing the hydrophilicity of membranes by grafting or blending with hydrophilic materials [16–18]; (iii) acquiring the optimum free volume characteristics or hydrophilic domains by manipulating membrane microstructure [19–22]. Among them, incorporating hygroscopic fillers into membranes has been demonstrated as a convenient and efficient approach. Recently, polymeric microcapsules were discovered to exhibit unique features in water retention. For instance, Wang et al. prepared imidazole polymeric microcapsules

* Corresponding author. Tel./fax: +86 22 23500086.
E-mail address: zhyjiang@tju.edu.cn (Z. Jiang).

0378-7753/$ – see front matter © 2013 Elsevier B.V. All rights reserved.
http://dx.doi.org/10.1016/j.jpowsour.2013.04.009

(IMCs) and embedded them into PEMs (e.g. sulfonated poly(ether ether ketone) (SPEEK)) to improve membrane water retention [13]. Compared with the control membrane, the composite membrane filled with 15 wt.% IMCs exhibited about seven times higher water retention and over ten times higher proton conductivity under relative humidity (RH) as low as 20%. For polymeric microcapsules, the functional groups on the shell played crucial roles in tuning water retention properties of the microcapsules and the membranes. In another study, Wang et al. synthesized three kinds of polymeric microcapsules with carboxylic acid, sulfonic acid, and pyridyl groups on the shell (designated as PMC-C, PMC-S, and PMC-N, respectively) [14]. Carboxylic acid group on the microcapsule shell possessed the highest hydration energy, which conferred the PMC-Cs and the PMC-C-filled membranes the highest bound-water content. As a result, the PMC-C-filled membranes displayed the lowest water release and the highest water retention, and hence the highest proton conductivity. In contrast, pyridyl group of PMC-Ns possessed the lowest hydration energy. Consequently, the PMC-N-filled membranes showed the lowest water retention and subsequently the lowest proton conductivity under identical conditions. It can be thus envisaged that developing polymeric microcapsules with both high water-retention and high proton conduction is essential to high performance PEM.

Although carboxylic acid group shows high water retention property, its intrinsic proton conductivity is low, due to its weak acidity and low dissociation (e.g. pKa = 4.19 for benzoic acid) [23]. In comparison, phosphonic acid group can also render superior water retention property [10], arising from its high binding energy [24]. Meanwhile, phosphonic acid group exhibits high self-dissociation and dissociation constant is 1.42 (phenylphosphonic acid), in turn conferring phosphonic acid-bearing materials higher Grotthuss-type proton conductivity than carboxylic acid-bearing materials [25,26]. In addition, phosphonic acid group possesses pronounced amphoteric properties, i.e. good proton donor and acceptor properties, accompanying with fast dynamic hydrogen-bond networks [25]. The above features may endow phosphonic acid group with high proton conductivity under the practical operating conditions of fuel cells. To the best of our knowledge, phosphonic acid polymeric microcapsules have rarely been exploited as the versatile fillers in PEMs.

In this study, phosphonic acid polymeric submicrocapsules (PASCs) were designed and synthesized via a facile distillation–precipitation polymerization [10,27,28]. The PASCs were then embedded into a SPEEK matrix for preparing a series of composite membranes. The compositions, structure and physicochemical properties of the PASCs and the membranes were characterized by Fourier transform infrared spectroscopy (FTIR), transmission electron microscopy (TEM), energy dispersive X-ray (EDX), field emission scanning electron microscope (FESEM), and thermogravimetric analysis (TGA). Water retention properties and proton conductivity of the PASCs and the membranes at 40 °C and 20% RH were evaluated. Furthermore, methanol barrier property of the membranes was investigated.

2. Experimental

2.1. Materials and chemicals

3-(Methacryloxy)propyltrimethoxysilane (MPS, 98%) and tetraethyl orthosilicate ($Si(OEt)_4$, TEOS, 98%) were provided by Aldrich Chemical Co., Inc. Ethyleneglycol dimethacrylate (EGDMA, 98%) and dimethyl vinylphosphonate (DMVP, 98%) were supplied by Alfa Aesar and purified by vacuum distillation. 2,2′-Azoisobutyronitrile (AIBN) as analytical grade was purchased from Tianjin and recrystallized from methanol. Acetonitrile (analytical grade, Tianjin Chemical Reagent II Co.) was dried with calcium hydride and purified by distillation prior to utilization. Hydrofluoric acid (HF, containing 40% of HF) was available from Tianjin Chemical Reagent Institute. Dimethylformamide (DMF), sulfuric acid and methanol were of analytical grade and used without any further purification. De-ionized water was used throughout the study.

2.2. Synthesis of the PASCs

Silica particles with different diameters were synthesized according to classical Stöber method [29] and the MPS-modified silica submicrospheres were obtained by coupling silica alcosol particles according to the literature [30]. A typical procedure for synthesizing core–shell phosphonate polymeric submicrospheres (PSs) with silica core and phosphonate shell was [27,28]: MPS-modified silica (0.30 g), EGDMA (0.60 mL), DMVP (1.00 mL), and AIBN (0.032 g) were dissolved in acetonitrile (80 mL) in a dried flask, attached with a fractionating column, Liebig condenser and a receiver. The reaction mixture was heated from room temperature till the boiling state within 10 min and the reaction mixture was kept under reflux state for further 10 min. After 40 mL acetonitrile was distilled off from the reaction system, the reaction was stopped and the resultant core–shell PSs were purified by repeated centrifugation, decantation, and resuspension in acetonitrile with ultrasonic-bathing for three times. The hybrid particles were immersed in 40% HF solution for 2 h. Then the excess HF and newly formed SiF_4 were expelled out by several centrifugation/washing cycles in water till the pH of 7. Subsequently, the synthesized phosphonate polymeric submicrocapsules were dispersed into excess HCl aqueous solution (10 mol L^{-1}) at 100 °C for 24 h. Three kinds of PASCs with lumen sizes of 128, 204 and 335 nm were obtained and designated as PASCs-1#, PASCs-2# and PASCs-3#, respectively. The resultant PASCs were finally dried in a vacuum oven at 50 °C until constant weight.

2.3. Preparation of SPEEK

PEEK (28 g) was dried at 60 °C till constant weight followed by dissolving in concentrated sulfuric acid (200 mL, H_2SO_4, 95–98 wt.%) with vigorous stirring at room temperature for 3 h and then at 45 °C for another 8 h. The sulfonation reaction was terminated by precipitating the polymer solution into water under continuous agitation. The precipitate was washed repeatedly with de-ionized water until the pH of 7, and then dried at room temperature for 2 days followed by drying at 60 °C for 24 h under vacuum. The degree of sulfonation (DS) of SPEEK was determined by acid–base titration.

2.4. Preparation of the membranes

An aliquot of PASCs were dispersed into DMF (3.0 mL) solution with ultrasonic treatment and stirred for 12 h. Simultaneously, SPEEK (0.7 g) was dissolved into DMF (4.0 mL) solution and stirred vigorously at room temperature for 24 h. Then, these two solutions were mixed under vigorous stirring for another 2 h. After degasification, the mixture was cast onto a clear glass plate and dried at 60 °C in a vacuum oven for 12 h, and then at 80 °C for another 12 h. After cooling down to room temperature, the membrane was peeled off from the glass plate. Then the membrane was immersed into 2.0 M H_2SO_4 solution for 2 days and rinsed with de-ionized water until the pH of 7, and then dried under vacuum at 60 °C. The composite membranes were designated as SPEEK/PASCs–*N*–*X*, where *N* (=1, 2, or 3 #) represented the type of the synthesized PASCs, and *X* (=2.5, 5, 10 or 15) was the weight percentage of the fillers to SPEEK. The SPEEK control membrane was also fabricated

for comparison purpose and designated as SPEEK. All the membranes in our study were of thickness in the range of 55–70 μm.

2.5. Characterizations

Transmission electron microscopy (TEM, Tecnai G2 20 S-TWIN) was used to detect the morphology of PASCs. Field emission scanning electron microscope (FESEM, Nanosem 430) was utilized to observe the morphology of the membranes after the membranes being freeze-fractured in liquid nitrogen and then sputtered with a thin layer of gold. Fourier transform infrared spectra (FTIR) of the samples were probed on a Bio-Rad FTS 135 instrument in the range of 4000–400 cm^{-1} with a resolution of 4 cm^{-1} at room temperature. The content of phosphorus of the PASCs was measured by EDX using FESEM. Zeta potential was detected using a Zeta PALS (Brookhaven Instrument Cooperation) through measuring the electrophoretic mobility of the PASCs at neutral pH and room temperature. Thermogravimetric analysis (TGA, NETZSCH-TG209F3) data of the samples was obtained from 40 to 800 °C with a heating rate of 10 °C min^{-1} under nitrogen flow.

2.6. Water uptake, water release, water retention and area swelling measurements

Before measurements, the samples were dried in a vacuum oven at 80 °C, the weight (W_{dry}) and area (A_{dry}) were measured. The samples were then immersed in deionized water at room temperature. The weight (W_{wet}) and area (A_{wet}) after complete hydration were measured. The final values of water uptake and area swelling were taken as the average of three measurements with an error within ±3.0% and calculated by Eqs. (1) and (2), respectively:

$$\text{Water uptake}\ (\%) = \frac{W_{wet} - W_{dry}}{W_{dry}} \times 100 \quad (1)$$

$$\text{Area swelling}\ (\%) = \frac{A_{wet} - A_{dry}}{A_{dry}} \times 100 \quad (2)$$

Then the samples were set in a climate box with a constant temperature and humidity of 40 °C and 20% RH and weighted at time t ($W_{wet\ t}$). Water release and water retention were calculated by Eqs. (3) and (4), respectively:

$$\text{Water release}\ (\%) = \frac{W_{wet} - W_{wet\ t}}{W_{wet} - W_{dry}} \times 100 \quad (3)$$

$$\text{Water retention}\ (\%) = \frac{W_{wet\ t} - W_{dry}}{W_{dry}} \times 100 \quad (4)$$

2.7. Methanol permeability

Methanol barrier property of the membranes was investigated using a glass diffusion cell consisting of two compartments with identical volume. The membrane was fully hydrated in water and then clamped tightly between two compartments. The two compartments were then filled with water and 2.0 M methanol solution, respectively. Under magnetic stirring, the methanol concentration in the water compartment was detected using a gas chromatography (Agilent 6820) equipped with a Thermal Conductivity Detector (TCD) and a DB624 column. Methanol permeability (P, $cm^2\ s^{-1}$) was the average of three measurements with an error within ±5.0% and calculated according to Eq. (5):

$$P = \frac{SV_B l}{AC_{A0}} \quad (5)$$

where S is the slope of the straight line of concentration versus time, V_B is the solution volume of the receipt compartment, l, A, and C_{A0} are the membrane thickness, effective membrane area and methanol feed concentration, respectively.

2.8. Ion-exchange capacity (IEC)

IEC of the samples was determined by acid–base titration. Samples were immersed in 2 M NaCl solution for at least 24 h to convert the H^+ ions into Na^+ ions. Then the solution was titrated using 0.01 M NaOH with phenolphthalein as indicator. The process was repeated three times and the IEC values with an accuracy of 0.01 mmol g^{-1} were obtained from the following Eq. (6):

$$\text{IEC}\left(\text{mmol g}^{-1}\right) = \frac{0.01 \times 1000 \times V_{NaOH}}{W_d} \quad (6)$$

where V_{NaOH} is the consumed volume of NaOH solution, and W_d is the dry weight of the samples.

2.9. Proton conductivity

Proton conductivity of the membrane was measured by the AC impedance spectroscopy method in vertical direction, and the membrane resistance was tested using a frequency response analyzer (FRA, Compactstat, IVIUM Tech.) with a potential of 20 mV in a frequency range of 10^6–1 Hz. The testing temperature was controlled by a climate box under 20 and 100% RH. To better analyze the function of water on proton transfer in the PEM, the measurement was conducted at low temperatures. The sample was completely hydrated in water prior to measurement. Proton conductivity (σ, S cm^{-1}) was calculated from the Eq. (7):

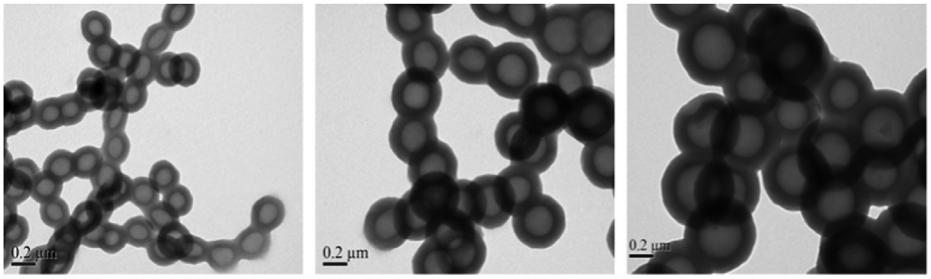

Fig. 1. TEM images of (a) PASCs-1#, (b) PASCs-2#, and (c) PASCs-3#.

$$\sigma = \frac{l}{AR} \quad (7)$$

where l, A, and R are the membrane thickness, the effective membrane area and the membrane resistance, respectively.

3. Results and discussion

3.1. Characterization of the PASCs

Three kinds of PACSs with similar shell thickness but different lumen sizes were synthesized, and their morphology was observed by TEM as depicted in Fig. 1. It could be found that the PASCs were clearly resolved by well-defined capsular configuration with dense shell and large lumen. The lumen sizes were 128 (PASCs-1#), 204 (PASCs-2#) and 335 nm (PASCs-3#), respectively, and the shell thickness for all the PASCs was about 85 nm, which was robust enough to preserve the hollow structure. The physicochemical properties of the PASCs were characterized by FTIR, EDX and TGA (Fig. 2). The presence of the functional groups on the shell was probed by FTIR in Fig. 2a. The characteristic peaks at about 1251 and 1154 cm^{-1} were assigned to the stretching vibration of P═O. The P–O bending vibration peak appeared at 967 cm^{-1} [31]. In addition, the peak at 1728 cm^{-1} was attributed to the C═O stretching vibration of the PASCs. The content of phosphorus was recorded by EDX in Fig. 2b and the calculated results were listed in Table 1. The phosphorus content was about 18.0 wt.% and the calculated phosphonic acid loading amount was about 47.1 wt.%, which was comparable to the literature results [32]. The surface chemical property was probed by Zeta PALS, which revealed that the zeta potential values were −51.82 (PASCs-1#), −52.54 (PASCs-2#) and −52.85 mV (PASCs-3#) (Table 1), respectively, suggesting that there were abundant electronegative charges on the PASCs surface. TGA traces of the PASCs in Fig. 2c showed a gradual weight loss from 150 °C, due to the reversible desorption of water produced by the self-condensation of phosphonic acid groups [33]. The major weight loss began at about 340 °C was attributed to the irreversible degradation of the C–P bond [33]. The above results indicated that three kinds of PASCs with controllable structure and abundant phosphonic acid groups on the shell were successfully synthetized.

3.2. Characterization of the membranes

The PASCs were incorporated into the SPEEK matrix to prepare composite membranes. The dispersion of submicrocapsules in the resultant composite membranes was analyzed using FESEM technique as shown in Fig. 3. Illustrative micrographs revealed that all the membranes were relatively dense and defect-free. The PASCs were uniformly dispersed into the SPEEK matrix, which was probably attributed to the electrostatic repulsive force between phosphonic acid groups during collision of the PASCs in the membrane casting solution [34]. Fig. 3b–e showed that the PASCs were partially broken during freeze-fracture in liquid nitrogen and the lumen could be clearly observed in the cross-section of the membranes.

FTIR spectra of the membranes were shown in Fig. 4. The characteristic peaks at 1214, 1072 and 1014 cm^{-1} were observed for all the membranes, which were assigned to the symmetric and asymmetric O═S═O stretching vibration of sulfonic acid groups [35,36], inferring the introduction of sulfonic acid groups. Compared with the SPEEK control membrane, a new characteristic peak at 1728 cm^{-1} was observed for the composite membranes, which corresponded to the C═O stretching vibration of the PASCs. The intensity of the peak became stronger with the increase of PASC content in the membranes.

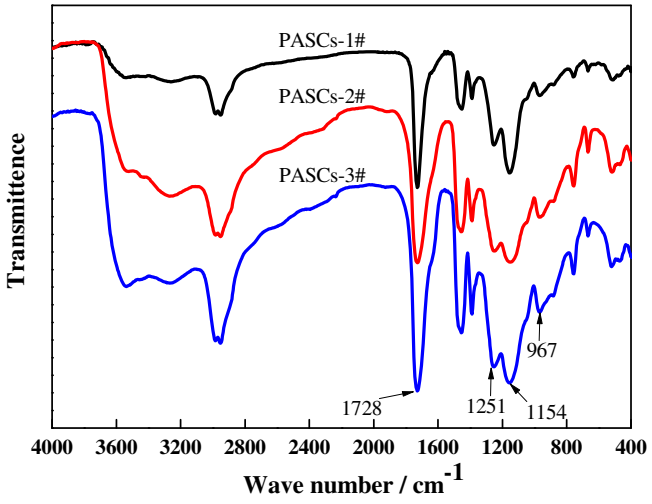

(a)

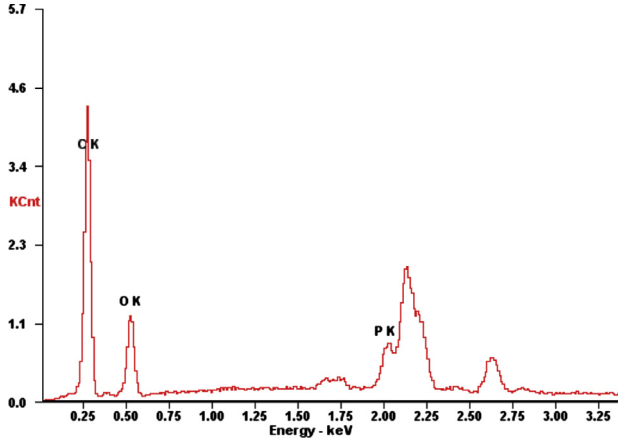

(b)

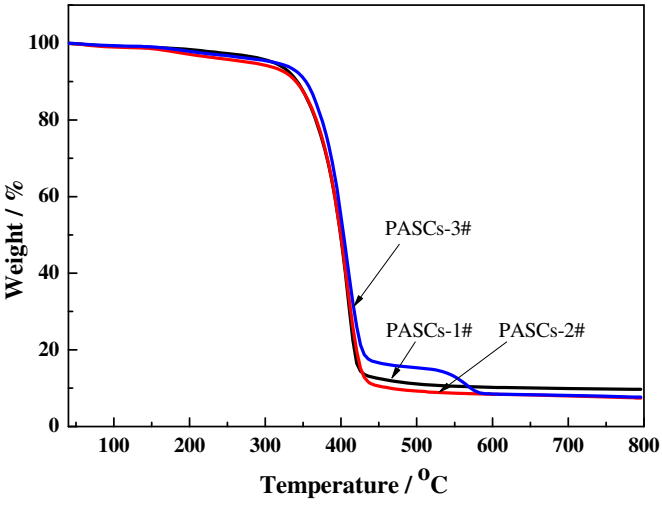

(c)

Fig. 2. (a) FTIR spectra, (b) EDX (PASCs-1#), and (c) TGA of the PASCs.

Table 1
The lumen size, shell thickness, IEC, zeta potential, water uptake, P content and $-PO_3H_2$ loading amount of the PASCs.

Sample	Lumen size (nm)	Shell thickness (nm)	IEC (mmol g^{-1})	Zeta potential (mV)	Water uptake (%)	P content (wt.%)	$-PO_3H_2$ loading amount (wt.%)
PASCs-1#	128 ± 3	72 ± 3	0.194	−51.82	212.9	17.8	46.6
PASCs-2#	204 ± 4	85 ± 3	0.193	−52.54	311.5	17.5	45.7
PASCs-3#	335 ± 5	90 ± 4	0.187	−52.85	384.3	18.0	47.1

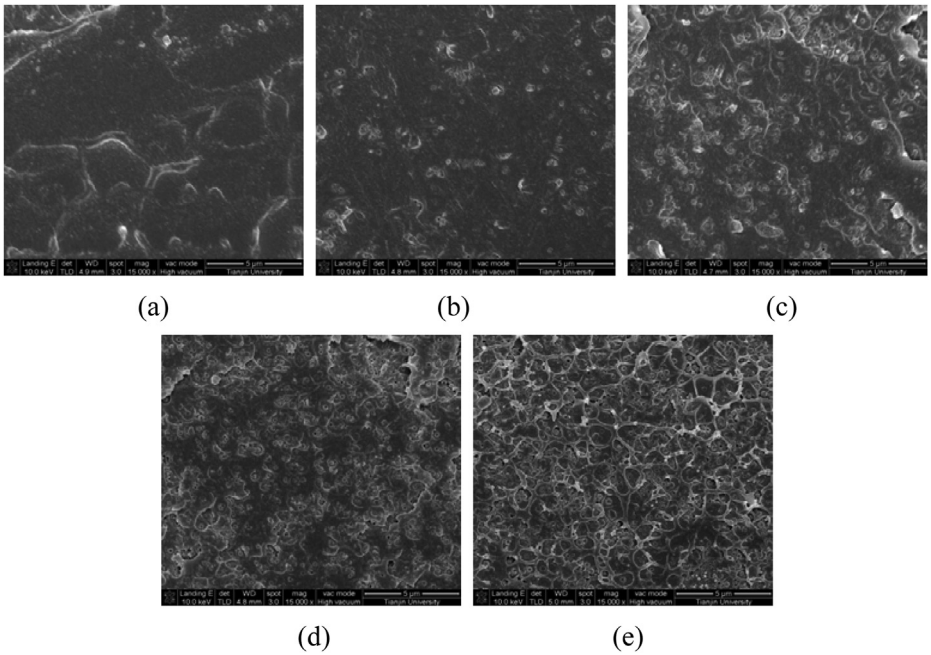

Fig. 3. FESEM images of the cross-section of (a) SPEEK, (b) SPEEK/PASCs-1#-2.5, (c) SPEEK/PASCs-1#-5, (d) SPEEK/PASCs-1#-10, and (e) SPEEK/PASCs-1#-15.

Fig. 5 showed the thermal stability of the membranes investigated by TGA. Three distinct weight loss steps were observed for all the membranes [37,38]: water evaporation (free and bound water) of the membranes (beginning at about 100 °C); the degradation of sulfonic acid groups (250–370 °C); the decomposition of the polymer chains (400–800 °C). At the end of the third region, the char yield of the composite membranes (e.g. 44.8–41.6% for the PASC-1#-filled membranes) was lower than that of the SPEEK control membrane (45.3%). It was probably due to the lower char yield of the incorporating PASCs-1# (9.7%) than that of the SPEEK chains (45.3%). It should be pointed out that the thermal stability of all the membranes was high enough (above 240 °C) to meet the temperature requirement for the practical application of fuel cells.

3.3. Water uptake and area swelling of the membranes

In the PEMs, adequate water is essential to efficient proton transfer via vehicle mechanism and Grotthuss mechanism [35].

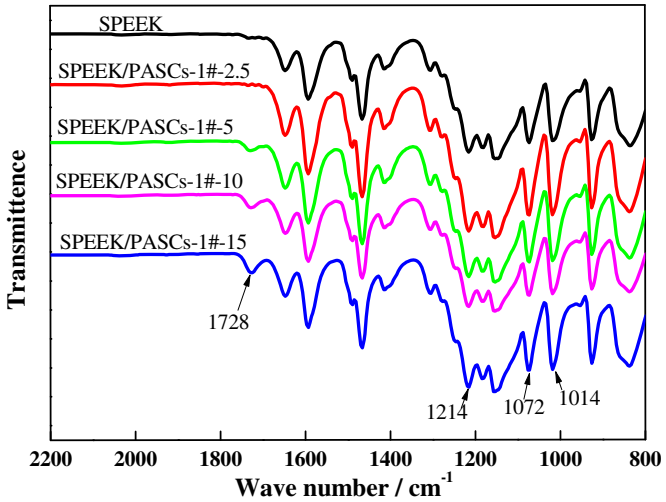

Fig. 4. FTIR spectra of the membranes.

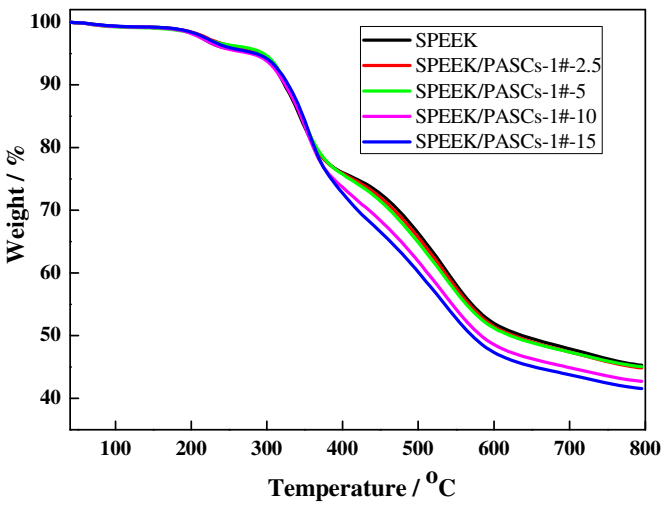

Fig. 5. TGA curves of the membranes.

Table 2
Water uptake, area swelling, IEC, methanol permeability, and proton conductivity of the membranes.

Entry	Membrane	Water uptake (%)[a]	Area swelling (%)	IEC (mmol g^{-1})	Methanol permeability (10^{-7} cm^2 s^{-1})	Proton conductivity (S cm^{-1})[a]
1	SPEEK	37.9	28.2	1.989	10.7	0.0173
2	SPEEK/PASCs-1#-2.5	52.1	27.3	1.962	10.6	0.0202
3	SPEEK/PASCs-1#-5	56.2	26.2	1.955	9.7	0.0218
4	SPEEK/PASCs-1#-10	58.0	25.2	1.890	8.3	0.0238
5	SPEEK/PASCs-1#-15	62.6	23.3	1.834	7.9	0.0251
6	SPEEK/PASCs-2#-2.5	53.4	27.3	1.964	10.4	0.0226
7	SPEEK/PASCs-2#-5	57.5	25.8	1.960	9.4	0.0251
8	SPEEK/PASCs-2#-10	60.3	24.1	1.872	8.3	0.0262
9	SPEEK/PASCs-2#-15	65.0	21.4	1.817	7.8	0.0268
10	SPEEK/PASCs-3#-2.5	54.3	27.2	1.956	10.3	0.0267
11	SPEEK/PASCs-3#-5	60.6	26.3	1.949	9.4	0.0277
12	SPEEK/PASCs-3#-10	62.8	24.7	1.868	8.0	0.0286
13	SPEEK/PASCs-3#-15	67.0	21.3	1.793	7.8	0.0292

[a] Water uptake and proton conductivity at 25 °C.

However, excess water content would lead to extreme membrane swelling, resulting in decreasing the dimensional and mechanical stability of the membrane. The water uptake and area swelling of the membranes were determined by measuring the changes in membrane weight and area, respectively (Table 2). The SPEEK control membrane displayed water uptake of 37.9% and area swelling of 28.2%. In comparison, the PASCs incorporation afforded enhanced water uptake but reduced area swelling to the composite membranes. For instance, with the PASC-1# content increasing from 2.5 to 15 wt.%, the water uptake of the composite membranes increased from 52.1 to 62.6%, whereas the area swelling decreased from 27.3 to 23.3%. Such phenomenon was reasonably ascribed to the following reasons: (i) the PASCs acting as reservoirs possessed high water uptake (e.g. 212.9% for PASCs-1#, Table 1) and hence rendered elevated water uptake for the PASC-filled membranes; (ii) the increased water was located within the submicrocapsules rather than the polymer bulk; and (iii) the incorporation of highly cross-linked PASCs possessed low swelling degree in the membranes. These results indicated that the water uptake enhancement of the composite membranes did not sacrifice their mechanical stability, and the trade-off between water uptake and swelling resistance of PEMs might be solved in such a facile way. For the PASCs with similar shell thickness, varying the lumen size from 128 to 335 nm made an increase of water uptake from 212.9 to 384.3% (Table 1). That should be attributed to the increased lumen volume per weight, which provided larger place for water storage. As a result, the water uptake of the PASC-filled composite membranes increased in the order of SPEEK/PASCs-1#-*X* < SPEEK/PASCs-2#-*X* < SPEEK/PASCs-3#-*X* under identical conditions.

3.4. Water release and water retention of the PASCs and the membranes

To investigate the function of water on proton transfer and explore the approach to high water-retention PEMs, the dynamic water release and water retention of the PASCs and the membranes at 40 °C and 20% RH were measured, as shown in Figs. 6 and 7. The relative water release slopes (Fig. 6a), suggested that the water loss rate of the PASCs increased with the lumen size increase. The slopes for PASCs-1#, PASCs-2#, and PASCs-3# were 0.0320, 0.0348 and 0.0447, respectively, and the water releases were 23.3, 25.0 and 32.4% after 700 min testing. It was ascribed to that when water was stored in a limited space, its vapor pressure obeyed Kelvin and Young–Laplace equations [19,39]. Therefore, larger lumen enhanced the vapor pressure and the consequent chemical potential of adsorbed water. Fortunately, three kinds of PASCs all showed relative slower water release rate when compared with other polymeric microcapsules (e.g. water release slopes of sulfonic

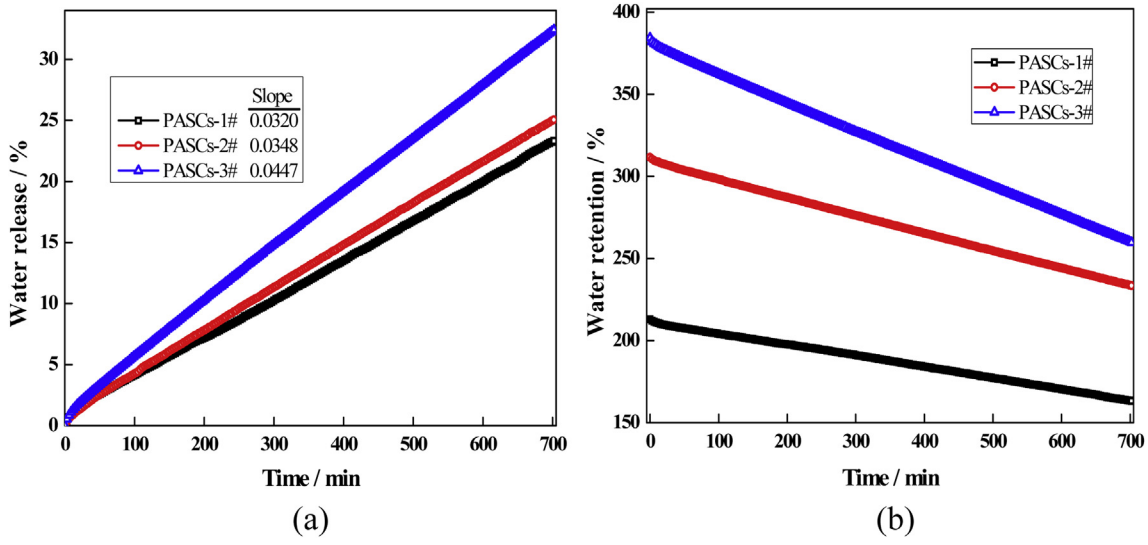

Fig. 6. (a) Water release, (b) water retention of the PASCs as a function of time at 40 °C and 20% RH.

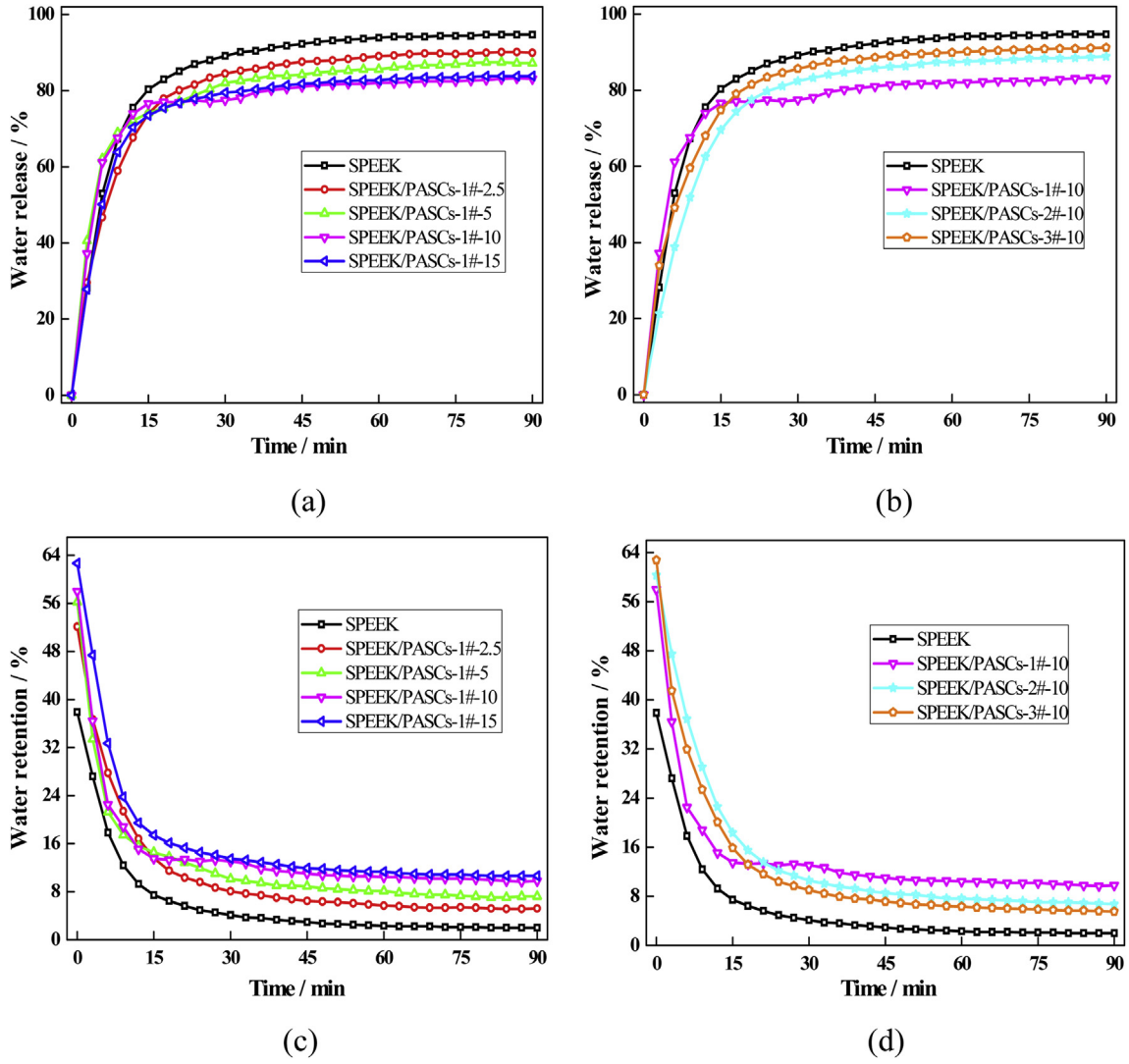

Fig. 7. (a), (b) Water release, and (c), (d) water retention of the membranes as a function of time at 40 °C and 20% RH.

acid and imidazole polymeric microcapsules being 0.055 and 0.053, respectively) [13,14]. Such results indicated that phosphonic acid on the PASCs had a strong affinity toward water molecules, thereby holding more water molecules in bound water state and retarding water release. Fig. 7a, b exhibited that water release of all the membranes, at 40 °C and 20% RH, followed similar processes: rapid evaporation of free water as the first step (0–30 min); slow water evaporation of bound water as the second step (from 33 to 90 min). The incorporating of PASCs retarded water release from 94.7% for the SPEEK control membrane to the range of 90.0–83.8% for the PASC-1#-filled membranes (Fig. 7a). For the three kinds of the PASC-filled composite membranes, the water release reduced in the order of SPEEK/PASCs-1#-*X* > SPEEK/PASCs-2#-*X* > SPEEK/PASCs-3#-*X* under the identical conditions (Fig. 7b), which was in agreement with the order of water loss rate of the fillers.

Water retention of the PASCs and the membranes was presented in Fig. 6b and Fig. 7c,d. Both water release rate and water uptake increased with the increase of the lumen size. As a result, PASCs-3# exhibited higher water retention than PASCs-1# within the testing time. For the membranes, the SPEEK control membrane suffered from fast water loss, resulting in the lowest water retention (2.0%) after 90 min testing. In comparison, the incorporation of PASCs significantly improved water retention properties of the membranes, and up to 10.6% water retention was obtained for the SPEEK/PASCs-1#-15 composite membrane. The elevated water retention properties of the composite membranes were ascribed to the high water-affinity of the PASCs wherein water molecules were fixed onto the shell by hydrogen bonds between water and phosphonic acid groups. During dehydration of the membranes under low humidity, the PASCs served as water reservoirs and continually released water into the membranes to maintain the bulk water environment. For the composite membranes, the SPEEK/PASCs-1#-*X* displayed higher water retention than SPEEK/PASCs-3#-*X* under identical conditions, most probably arising from the lower water loss rate of the PASCs-1#.

3.5. IEC and proton conductivity of the membranes

IEC was an important parameter for directly reflecting the available proton-conducting sites in PEMs. High IEC, indicating the more proton carrier sites of the membrane, was necessary for high proton conductivity. IEC values of the samples were determined by titration, as shown in Tables 1 and 2. The IEC of the SPEEK control membrane was 1.989 mmol g^{-1}. In comparison, increasing the PASC-1# content from 2.5 to 15 wt.% decreased the membrane IEC from 1.962 to 1.834 mmol g^{-1}. Such phenomenon can be attributed

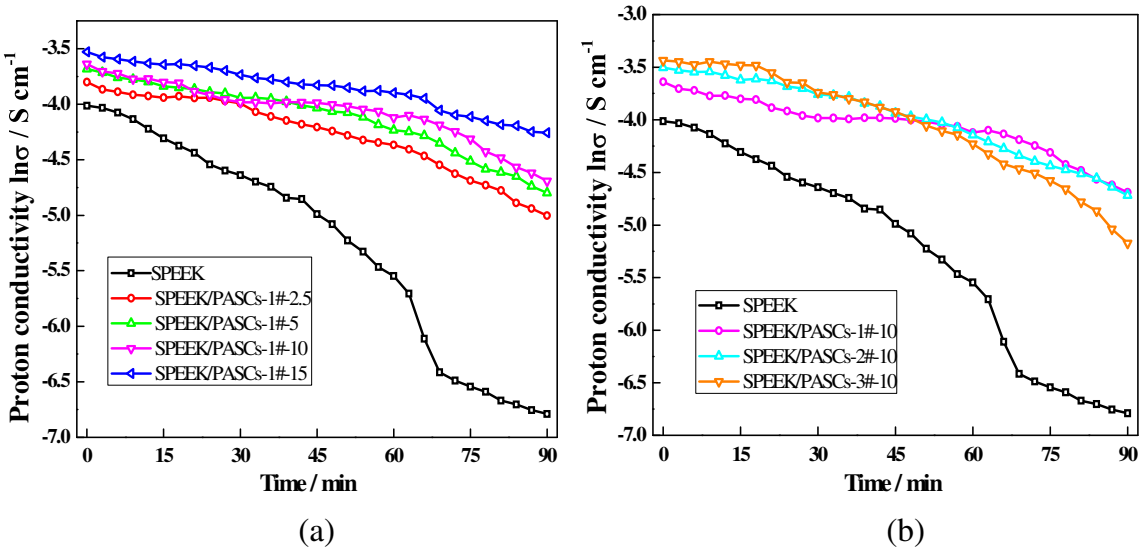

Fig. 8. (a), (b) Proton conductivity of the membranes as a function of time at 40 °C and 20% RH.

to the incorporation of PASCs, which diluted the concentration of sulfonic acid groups due to lower IEC values compared with SPEEK chains.

Proton conductivity was one of the critical parameters for a PEM and high proton conductivity could afford a fuel cell high operational fuel cell voltage and current output. The proton conductivity of the membranes was listed in Table 2. The SPEEK control membrane showed a proton conductivity of 0.0173 S cm^{-1} at 25 °C and 100% RH. In comparison, incorporating PASCs enhanced the proton conductivity of the composite membranes. For example, increasing the PASC-1# content from 2.5 to 15 wt.% elevated the proton conductivity from 0.0202 to 0.0251 S cm^{-1}. Moreover, the proton conductivity of the SPEEK/PASCs-3#-*X* composite membrane was higher than that of the SPEEK/PASCs-1#-*X* composite membrane with the same filler content. The enhancement in proton conductivity could be interpreted as follows: (i) although the PASCs incorporation reduced the membrane IEC values, which might reduce Grotthuss-type proton transfer, the PASCs elevated water uptake of the membranes, which increased proton conductivity via vehicle mechanism by increasing hydronium ions and via Grotthuss mechanism by dissociating sulfonic acid groups; (ii) amphoteric phosphonic acid groups on the PASC shell could also offer fast proton hopping by forming hydrogen-bond networks. The above results indicated that the proton conductivity showed stronger dependence on water content than the IEC values and the filler sizes in the membranes at 25 °C and 100% RH.

To better correlate water retention and proton conductivity, proton conductivity as a function of time at 40 °C and 20% RH was measured. Fig. 8 revealed that all the membranes displayed a decline in proton conductivity within the testing time, which further manifested that the strong dependence of proton conductivity on water in the membranes. The proton conductivity of the SPEEK control membrane declined significantly from 0.0181 to 0.0011 S cm^{-1} after 90 min testing, with a reduction of 94%. Encouragingly, the PASC-filled composite membranes exhibited slower reduction in proton conductivity. For instance, the proton conductivity was only reduced by 70% (from 0.0223 to 0.0067 S cm^{-1}), 67% (from 0.0251 to 0.0082 S cm^{-1}), 65% (from 0.0263 to 0.0092 S cm^{-1}), and 52% (from 0.0293 to 0.0142 S cm^{-1}) when 2.5–15 wt.% PASCs-1# were incorporated. The elevated water retention of membranes might account for the high proton conductivity under low humidity. Meanwhile, the high degree of self-dissociation and amphoteric features of phosphonic acid groups might assist Grotthuss-type proton transfer by offering the dynamic hydrogen-bond networks under low humidity, even in anhydrous state.

3.6. Methanol permeability of the membranes

Due to its high cell efficiency, simple system design and low environmental pollution, the direct methanol fuel cell (DMFC) has stimulated great interest as one kind of promising PEMFC [40]. To diminish the mixed potential effect and catalyst poisoning, a good methanol barrier property (methanol permeability $< 10^{-6}$ cm^2 s^{-1}) is essentially desired for the PEM used in a DMFC [41]. In order to explore methanol barrier property of the composite membranes, the methanol permeability of the membranes at room temperature was measured and the results were listed in Table 2. The methanol permeability of the SPEEK control membrane was 10.7×10^{-7} cm^2 s^{-1}, which was much lower than that of Nafion 117 (31.4×10^{-7} cm^2 s^{-1}) [34]. Compared with the SPEEK control membrane, the composite membranes displayed improved methanol barrier property. Increasing the filler content could endow the composite membranes with gradually decreased methanol permeability (e.g. $10.6–7.9 \times 10^{-7}$ cm^2 s^{-1} for the PASC-1#-filled membranes). The improvement of methanol barrier property should be ascribed to the presence of the highly cross-linked PASCs, which prolonged the pathways of methanol transport and increased the methanol diffusion barrier. Similar observations have been reported in other microcapsule-filled composite membranes [15].

4. Conclusion

In this study, phosphonic acid polymeric submicrocapsules with tunable lumen sizes were synthesized and incorporated into the SPEEK matrix to prepare composite membranes. The PASCs served at least dual functions: the lumen and the shell of the submicrocapsules endowed the membranes with enhanced water uptake and water retention properties; the phosphonic acid groups on the shell introduced adequate amphoteric proton carriers, and

thus enhanced the proton transfer via vehicle and Grotthuss mechanisms. Consequently, the PASC-filled composite membranes acquired higher proton conductivity than the SPEEK control membrane. In particular, the composite membrane filled with 15 wt.% PASCs-1# exhibited the highest proton conductivity of 0.0142 S cm^{-1} at 40 °C and 20% RH after 90 min testing, about twelve times higher than that of the SPEEK control membrane. Moreover, the composite membranes showed lower methanol permeability ($10.6–7.9 \times 10^{-7}$ cm^2 s^{-1}) than Nafion 117 (31.4×10^{-7} cm^2 s^{-1}). Considering their facile, controlled synthesis procedure, superior water retention and proton conduction properties, the PASCs may be utilized as an efficient water-retention and proton-conduction materials in diverse energy and environment relevant fields.

Acknowledgments

We gratefully acknowledge financial support from National Science Fund for Distinguished Young Scholars (21125627), the National High Technology Research and Development Program of China (2012AA03A611), and the Program of Introducing Talents of Discipline to Universities (No. B06006). Thanks prof. Xinlin Yang, Nankai University, China and Dr. Jingtao Wang, Zhengzhou University, China for their valuable help in this study.

References

[1] M. Ahmed, I. Dincer, Int. J. Energy Res. 35 (2011) 1213–1228.
[2] K.D. Kreuer, Chem. Mater. 8 (1996) 610–641.
[3] T.J. Peckham, S. Holdcroft, Adv. Mater. 22 (2010) 4667–4690.
[4] T.A. Zawodzinski, J. Dawy, J. Valerio, S. Gottesfeld, Electrochim. Acta 40 (1995) 297–302.
[5] B.J. Siwick, H.J. Bakker, J. Am. Chem. Soc. 129 (2007) 13412–13420.
[6] C. Bi, H. Zhang, Y. Zhang, X. Zhu, Y. Ma, H. Dai, S. Xiao, J. Power Sources 184 (2008) 197–203.
[7] I. Nicotera, A. Enotiadis, K. Angjeli, L. Coppola, G.A. Ranieri, D. Gournis, J. Phys. Chem. B 115 (2011) 9087–9097.
[8] M.K. Mistry, N.R. Choudhury, N.K. Dutta, R. Knott, Z. Shi, S. Holdcroft, Chem. Mater. 20 (2008) 6857–6870.
[9] Y. Jin, S. Qiao, L. Zhang, Z.P. Xu, S. Smart, J.C. Diniz da Costa, G.Q. Lu, J. Power Sources 185 (2008) 664–669.
[10] L. Nie, J. Wang, T. Xu, H. Dong, H. Wu, Z. Jiang, J. Power Sources 213 (2012) 1–9.
[11] H. Pu, D. Wang, Z. Yang, J. Membr. Sci. 360 (2010) 123–129.
[12] D.-H. Son, R.K. Sharma, Y.-G. Shul, H. Kim, J. Power Sources 165 (2007) 733–738.
[13] J. Wang, X. Yue, Z. Zhang, Z. Yang, Y. Li, H. Zhang, X. Yang, H. Wu, Z. Jiang, Adv. Funct. Mater. 22 (2012) 4539–4546.
[14] J. Wang, H. Zhang, X. Yang, S. Jiang, W. Lv, Z. Jiang, S.Z. Qiao, Adv. Funct. Mater. 21 (2011) 971–978.
[15] J. Wang, Z. Zhang, X. Yue, L. Nie, G. He, H. Wu, Z. Jiang, J. Mater. Chem. A 1 (2013) 2267–2277.
[16] V.A. Deimede, J.K. Kallitsis, Macromolecules 38 (2005) 9594–9601.
[17] M.N.A. Mohd Norddin, A.F. Ismail, D. Rana, T. Matsuura, S. Tabe, J. Membr. Sci. 328 (2009) 148–155.
[18] M.N.A. Mohd Norddin, A.F. Ismail, D. Rana, T. Matsuura, A. Mustafa, A. Tabe-Mohammadi, J. Membr. Sci. 323 (2008) 404–413.
[19] M.J. Park, K.H. Downing, A. Jackson, E.D. Gomez, A.M. Minor, D. Cookson, A.Z. Weber, N.P. Balsara, Nano Lett. 7 (2007) 3547–3552.
[20] R. Guo, O. Lane, D. VanHouten, J.E. McGrath, Ind. Eng. Chem. Res. 49 (2010) 12125–12134.
[21] D. Chen, S. Wang, M. Xiao, Y. Meng, A.S. Hay, J. Mater. Chem. 21 (2011) 12068–12077.
[22] K. Nakabayashi, T. Higashihara, M. Ueda, Macromolecules 44 (2011) 1603–1609.
[23] H. Levitan, J. Barker, Science 176 (1972) 423–425.
[24] S.J. Paddison, K.D. Kreuer, J. Maier, Phys. Chem. Chem. Phys. 8 (2006) 4530–4542.
[25] M. Schuster, T. Rager, A. Noda, K.D. Kreuer, J. Maier, Fuel Cells 5 (2005) 355–365.
[26] R.G. Franz, AAPS PharmSci 3 (2001) 1–13.
[27] G. Liu, H. Zhang, X. Yang, Y. Wang, Polymer 48 (2007) 5896–5904.
[28] G. Li, Q. Shi, S.J. Yuan, K.G. Neoh, E.T. Kang, X. Yang, Chem. Mater. 22 (2010) 1309–1317.
[29] W. Stöber, A. Fink, J. Colloid Interface Sci. 26 (1968) 62–69.
[30] E. Bourgeat-Lami, J. Lang, J. Colloid Interface Sci. 197 (1998) 293–308.
[31] S.H. Kim, Y.C. Park, G.H. Jung, C.G. Cho, Macromol. Res. 15 (2007) 587–594.
[32] J. Parvole, P. Jannasch, Macromolecules 41 (2008) 3893–3903.
[33] J. Parvole, P. Jannasch, J. Mater. Chem. 18 (2008) 5547–5556.
[34] J. Wang, H. Zhang, Z. Jiang, X. Yang, L. Xiao, J. Power Sources 188 (2009) 64–74.
[35] J. Devaux, D. Delimoy, D. Daoust, R. Legras, J.P. Mercier, Polymer 26 (1985) 1994–2000.
[36] P. Xing, G.P. Robertson, M.D. Guiver, S.D. Mikhailenko, K. Wang, S. Kaliaguine, J. Membr. Sci. 229 (2004) 95–106.
[37] K.N.T. Do, D. Kim, J. Power Sources 185 (2008) 63–69.
[38] Y. Zhang, H. Zhang, Y. Zhai, X. Zhu, C. Bi, J. Power Sources 168 (2007) 323–329.
[39] S. Moghaddam, E. Pengwang, Y.-B. Jiang, A.R. Garcia, D.J. Burnett, C.J. Brinker, R.I. Masel, M.A. Shannon, Nat. Nanotechnol. 5 (2010) 230–236.
[40] C.-K. Lin, J.-C. Tsai, J. Mater. Chem. 22 (2012) 9244–9252.
[41] S.P. Jiang, Z. Liu, Z.Q. Tian, Adv. Mater. 18 (2006) 1068–1072.